ORIGINAL ARTICLE

Ring Artefact as a Potential Intrinsic Feature in CT Imaging: A Phantom-Based Study

Akpama Egong [1*], Blessing Ibe [1], Akwa Erim [1], Emmanuel Owolo [2], Nneoyi Egbe [1], Chamberlain Uket [3]

[1] *Department of Radiography and Radiological Science, University of Calabar, Calabar, Nigeria*

[2] *Tip Top Dignostic Center, Aduwawa, Benin, Nigeria*

[3] *Liverpool Heart and Chest Hospital, UK*

*Corresponding Author: Akpama Egong

Email: akpamaegong@unical.edu.ng

Received: 20 November 2025 / Accepted: 16 June 2026

Abstract

Purpose: Defective tube or miscalibration has been implicated as the causes of Computed Tomography (CT) ring artifacts, implying that images acquired with such scanner should demonstrate ‘’ring(s)’’ artefact. However, ‘’ring(s)’’ artefact is frequently seen in moderate to severe hydrocephalic images but lacking on non-hydrocephalic images acquired using same machine. Hence we investigate causes of persisting ‘’ring(s)’’ artifact demonstrable on hydrocephalic CT images.

Materials and Methods: The research included hydrocephalic and hydrocdphalous mimicking phantom CT images with ‘’ring’’ band(s) designated as inner, middle and outer band, and non-hydphalous CT image without ‘’ring’’ band divided into four quadrants - Anterior Right (AR), Anterior Left (AL), posterior right (PR), and Posterior Left (PL). The CT number was measured at four perpendicular points per ‘’ring’’ and randomly at four points in each quadrant. CT number measurement was carried out using DICOM image viewer version 22504.418.1.0., Region of Interest (ROI) = 0.10cm^2), and with the outermost ‘’ring’’ band taken control, the relationships between CT number mean values between ‘’ring’’ band, and each quadrant was analyzed.

Results: Dunnette multiple comparison test shows a significant difference in CT numbers between the Inner, Middle and Outer ‘’ring’’ bands with mean pixel values -1.194, -3.167, and 0.007 for hydrocephalous mimicking phantom image. Substantial difference in CT numbers between the Outer and Middle ‘’ring’’ band and similarity between the Outer and Inner ‘’ring’’ band on hydrocephalic image was also found with mean pixel values of 2.444, -1.593 and 2.222. For the non-hydrocephalic images, similarity in CT numbers across the four quadrants was noted with mean pixel values of AR = 17.89, AL=18.56, PR=17.17, and PL=14.00.

Conclusion: CT ring artefacts may be patient based, indicating onset of pathologic process and diagnostic indicator.

Keywords: Computed Tomography Number; Ring Artifact; Photon Starvation; Beam Hardening; Hydrocephalus.

DOI:

Frontiers in BIOMEDICAL TECHNOLOGIES

1. Introduction

Generally, an artefact can be termed as a distortion or flaw in an image which does not relate to the subject under examination. For Computed Tomography (CT), this can be redefined as anything misread by the detectors that results in the assignment of an incorrect Computed Tomography number (CTn) value. That is, systematic deviation between the CTn in the image formed and the real attenuation coefficients of the scan subject [1].

CT image is composed of a matrix of picture elements (pixels), the scanned subject can be considered as being made up of a matrix of differential linear attenuation coefficient volume elements (voxels). The attenuation value stored in each picture element is known as the Hounsfield Units (HU) or CT number (CTn), representing the average linear attenuation coefficient of tissues (μt), in the volume element varying within an approximate range -1000 to +3000 [2,3].

It is assumed that, except for water and air, variations in the HU values for all substances determined at differential tube voltages (kVp) and temperatures will occur. This variation can also be a function of photon energy, and thus, different substances will demonstrate a non-linear relation of their attenuation coefficient with respect to that of water [3]. Such variation of CTn with tube kVp is due to tissue heterogeneity and filtration of the X-ray beam. This means that as x-radiation passes through the subject, there is differential absorption of x-radiation by the tissues of the subject, and the emergent x-ray beam from the subject carries a pattern of intensity that is influenced by the thickness and composition of the tissue in the subject [2].

The assigned pixel values in a CT image are related to the attenuation of the corresponding tissue, or, more precisely, to their linear attenuation coefficient μ (m^{-1}), which is dependent on the x-ray beam photon energy, the make-up of the subject, and the density of the material. Therefore, CT may be prone to artefact formation due to any error or discrepancy in measured pixel values originating from sources like the physical processes used in CT data acquisition, CT scanner components, and the patient [4, 3].

CT ‘’ring’’ artifact is a concentric ring(s) bands with varying intensities that appear superimposed on the image and interfere with image analysis and remain a problem in CT image acquisition [5, 3]. Despite advances in CT technology, the " ring " artefact, among others persist and studies in the CT imaging domain have implicated defective tube and/or tube miscalibration as the sole causes of ring artefact on CT images of the skull [6]. In practice, however, ring artifact has been observed only consistently, especially on images of water phantom and moderate-to-gross paediatric hydrocephalus cases – a medical condition indicative of cerebrospinal fluid volume in excess of 150 ml [7- 12] and not on non-hydrocephalus images. It is unclear what really accounts for the formation of these rings, and the implicated causes in the literature appear to be inadequate in explaining the causes, since the rings do not appear universally on all images produced under similar protocols and conditions, hence this study.

2. Materials and Methods

CT images of phantom mimicking moderate-to-gross paediatric hydrocephalus (Figure 2a and 2b), moderate paediatric hydrocephalus with a ’ ring ’ band (Figure 3), and non-hydrocephalus head without ‘ring’ (Figure 4) were used for this study.

The moderate-to-gross paediatric hydrocephalus mimicking phantom was constructed as follows:

i. A Perspex sheet 4mm thick as Cranium Simulating Tissue (CST) [13] was cut to size 38cm x 6 cm (length and breadth) to yield the desired 13.00 cm equivalent internal diameter of the phantom when folded into shape. This represents the effective diameter of the head for the paediatric age range (0 – 2 years) under study.

The dimension of the skull vertex to the base of the skull was not incorporated into phantom construction since x-rays traverse the antero-posterior and biparietal diameters representing the effective head diameter during CT head image acquisition.

ii. The Perspex sheet was heated over Microwave oven at medium power level (50-70%) intermittently for 0-5 minutes at intervals of 5 seconds – an attempt aimed at reducing the Perspex hardness, rendering it

workable into the desired cylindrical shape by folding and tying it over a cylindrical pipe.

iii. Immediate cooling of the cylindrically shaped Perspex achieved by immersion in water at room temperature (27^0C) for 2 hours to ensure uniform wall thickness and prevent wall cracks due to uneven contraction of the heated Perspex sheet was undertaken.

iv. Following the cooling phase, cut-to-size circular Perspex sheets (13.5 cm in dimension) were aligned to enclose both ends of the formed Perspex cylinder using registration marks (a, b, c, and d) and then glued together sequentially using wood glue to form a hollow compartment. Wood glue has been found to behave radiologically similar to soft tissue at diagnostic x-ray energies [14].

v. After allowing the assembly to set for 30 minutes, the excess wood glue was removed carefully with a razor blade, and the phantom was filled with distilled water through the drilled slit to mimic a gross paediatric hydrocephalic environment (Figure 1).

Figure 1a. Head Phantom mimicking moderate-to-severe hydrocephalus

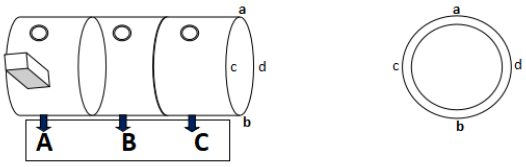

Figure 1b. Schematic diagram of a Head Phantom mimicking moderate-to-severe hydrocephalus

vi. A General Electric (GE) Brivo light-speed 16-slice CT scanner (Model number – CT 385;

Tube type – MX-135, Manufacturer – General electric (GE); Date of manufacture – 2012

was used to acquire phantom images using the paediatric protocol/parameters.

vi. Observed varying intensities describing concentric paths on the paediatric hydrocephalus and phantom mimicking hydrocephalus images were designated as Inner, Middle and Outer ‘’ring’’ bands, with Outer ‘’ring’’ band selected as a control (Figure 2).

CT image of a non-hydrocephalic head without ‘ring’ was divided into four equal quadrants designated as Anterior Right (AR), Anterior Left (AL), Posterior Right (PR), and Posterior Left (PL), and CTn was taken randomly at four points in each quadrant for images of a normal paediatric head. Since each region is assumed to have a similar attenuation coefficient, evident by the homogeneous appearance of the regions, the CT number was measured at four perpendicular points on each ‘’ring’’ band on images of paediatric hydrocephalus and phantom mimicking hydrocephalus, and per quadrant on non-hydrocephalus image was to obtain the average pixel value. CT number extraction was carried out using DICOM image viewer version 22504.418.1.0, with region of interest (ROI) = 0.10 cm^2.

2.1. Data Analysis

Normality test revealed data set to be normally distributed. The mean values between ‘’ring’’ bands, and among quadrants were compared using Dunnett’s test. Statistical analysis was performed using the Minitab statistical software version 17. Statistical significance was set at $p \leq 0.05$.

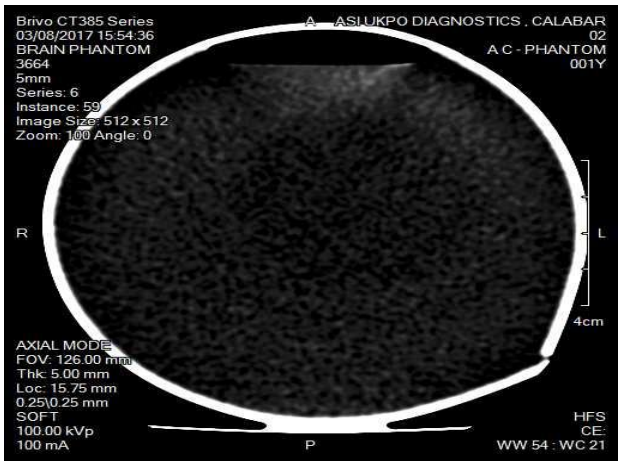

Figure 2a. Phantom mimicking moderate-to-gross paediatric hydrocephalus: Axial plane

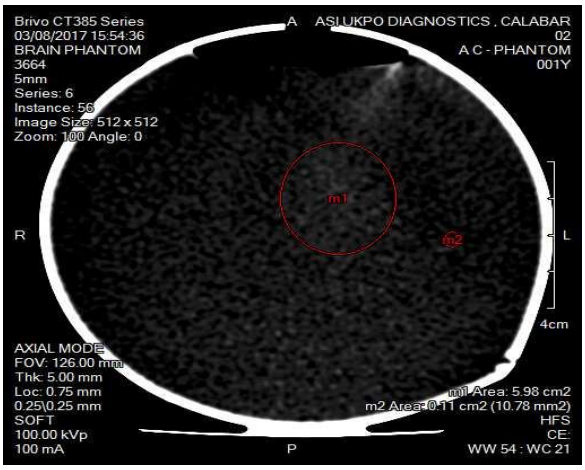

Figure 2b. Phantom mimicking moderate-to-gross paediatric hydrocephalus with ROI (small red circle)

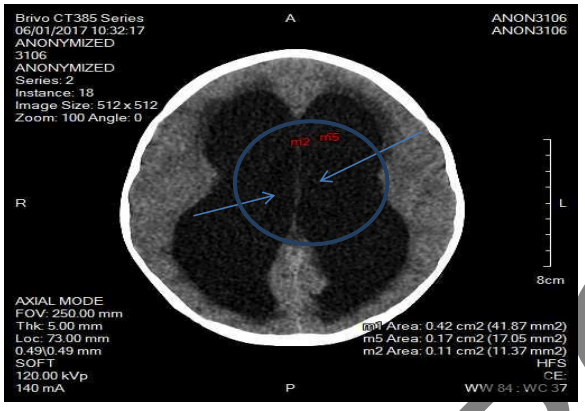

Figure 3. Paediatric hydrocephalus images with ring artefacts as indicated by arrows

3. Results

The mean CTn number of the ‘ring’’ bands (Inner, Middle, and Outer) are -1.194, -3.167, and 0.007, respectively (Table 3) for phantom mimicking hydrocephalus images. Significant differences exist between the ‘’ring’’ bands (Table 6). This connotes that the middle and inner layers vary significantly with the outermost layer, supporting the presence of three ‘’ring’’ bands of significant intensity difference as demonstrated and distinguished with good contrast on the image (Figure 2a). Ring Bands are visually observed on moderate paediatric hydrocephalus Images. However, significant differences exist only between the middle and outer layers with mean CTn (Inner = 2.222, Middle = -1.593, Outer = 2.444) (Table 4). This suggests that only the middle and inner layers vary with significant intensity brightness (Table 7). Similarity in CTn was seen across the non-hydrocephalus head image quadrants (Table 8). This relates to the difference in intensity, describing a circular path is nonexistent as visually observed (Figure 4).

The Table 3 indicates the mean and standard deviation values for inner, middle, and outer regions in a severe hydrocephalus phantom image.

Table 1. Protocol for paediatric head mimicking phantom CT scan

Parameter	Measurement
Slice thickness	5.00 mm
Table increment	7 mm
kiloVoltage power	100 kVp
mAs per slice	100 mAs
Algorithm	soft
Scan field of view	126 mm
Scan mode	axial
Window width	54
Window level	21

Table 2. Phantom mimicking moderate-to-gross paediatric hydrocephalus CT IMAGE acquisition protocol

PARAMETER	MEASUREMENT
kVp,	100 kVp,
mAs	100 mAs
tube current modulation settings (if used),	
Rotation time	0.3 s
Pitch	0.5625:1
Detector configuration	24-row helical HiLight Scintillator Detector
Slice thickness	5.00 mm
Increment reconstruction	0.625 mm
kernel/filter,	Volumetric Image Space Reconstruction (**VISR) 3D filter**
Reconstruction algorithm (FBP/IR and	**Adaptive Statistical Iterative Reconstruction (ASiR), VERSION: Original**
name/version)	
Matrix size	512 x 512
Field of view (FOV)	126 00 mm
Window/level used for measurements	21

Table 3. Descriptive statistics of pixel values of the regions in the severe Hydrocephalus phantom image

Factor	N	Mean	StDev	95% CI
Inner	144	-1.194	2.419	(-1.586, -0.802)
Middle	144	-3.167	2.626	(-3.559, -2.775)
Outer	144	0.007	2.107	(-0.385, 0.399)

Table 4. Descriptive statistics of pixel values of the regions in the moderate paediatric hydrocephalus image

Factor	N	Mean	StDev	95% CI
Inner	27	2.222	1.502	(1.526, 2.919)
Middle	27	-1.593	2.024	(-2.289, -0.896)
Outer	27	2.444	1.888	(1.748, 3.141)

The Table 4 indicates the mean and standard deviation values for inner, middle, and outer regions in a moderate paediatric hydrocephalus image.

Table 5. Descriptive statistics of pixel values of the regions in paediatric non-hydrocephalus image

Factor	N	Mean	StDev	95% CI
A + AR	18	17.89	7.72	(14.29, 21.49)
R + PR	18	17.17	8.56	(13.57, 20.77)
P + PL	18	14.00	7.84	(10.40, 17.60)
L + AL	18	18.56	6.33	(14.95, 22.16)

The Table 5 above indicates the mean and standard deviation values for inner, middle, and outer regions in paediatric non-hydrocephalus image.

The outer regions demonstrate significantly higher pixel values than the inner and middle regions ($p = 0.001$).

The pixel values for the inner and outer regions are statistically the same ($p = 0.864$). The outer region has statistically higher values than the middle region ($p = 0.001$.

The Table 8 shows that there is no difference in pixel values between the quadrants ($p > 0.05$)

4. Discussion

This study was carried out to demonstrate ring bands on images of a homogeneous or relatively homogeneous unit and to determine their CTn values for each visually perceived ring band on acquired image(s) from such a unit. Measurement of CTn values for ring bands present in moderate to severe hydrocephalus head images with rings and per quadrant in mild to nil paediatric hydrocephalus head images was also taken. The study shows the formation of ring bands in the phantom unit images as well as

Table 6. Dunnett's Simultaneous Tests for Level Mean - Control Mean for measured pixel values for observed ring intensities: on paediatric hydrocephalic mimicking phantom images

Difference of Level	Difference of Means	SE of Difference	95% CI	Adjusted T Value	P-Value
Inner – Outer	-1.201	0.282	(-1.825, -0.577)	-4.26	0.001
Middle - Outer	-3.174	0.282	(-3.798, -2.550)	11.25	0.001

Table 7. Dunnett's Simultaneous Tests for Level Mean - Control Mean for Measured pixel values for observed ring intensities: on paediatric hydrocephalic images

Difference of Level	Difference of Means	SE of Difference	95% CI	Adjusted T Value	P-Value
Inner – Outer	0.222	0.495	(-1.337, 0.893)	-0.45	0.864
Middle - Outer	-4.037	0.495	(-5.152, -2.922)	-8.16	0.001

Table 8. Dunnett's Simultaneous Tests for Level Mean - Control Mean for Measured pixel values for observed ring intensities: non-hydrocephalic images without rings seen

Difference of Level	Difference of Means	SE of Difference	95% CI	Adjusted T Value	P-Value
PR - AR	-0.72	2.55	(-6.85, 5.41)	-0.28	0.985
PL – AR	-3.89	2.55	(-10.02, 2.24)	-1.52	0.301
AL - AR	0.67	2.55	(-5.47, 6.80)	0.26	0.988

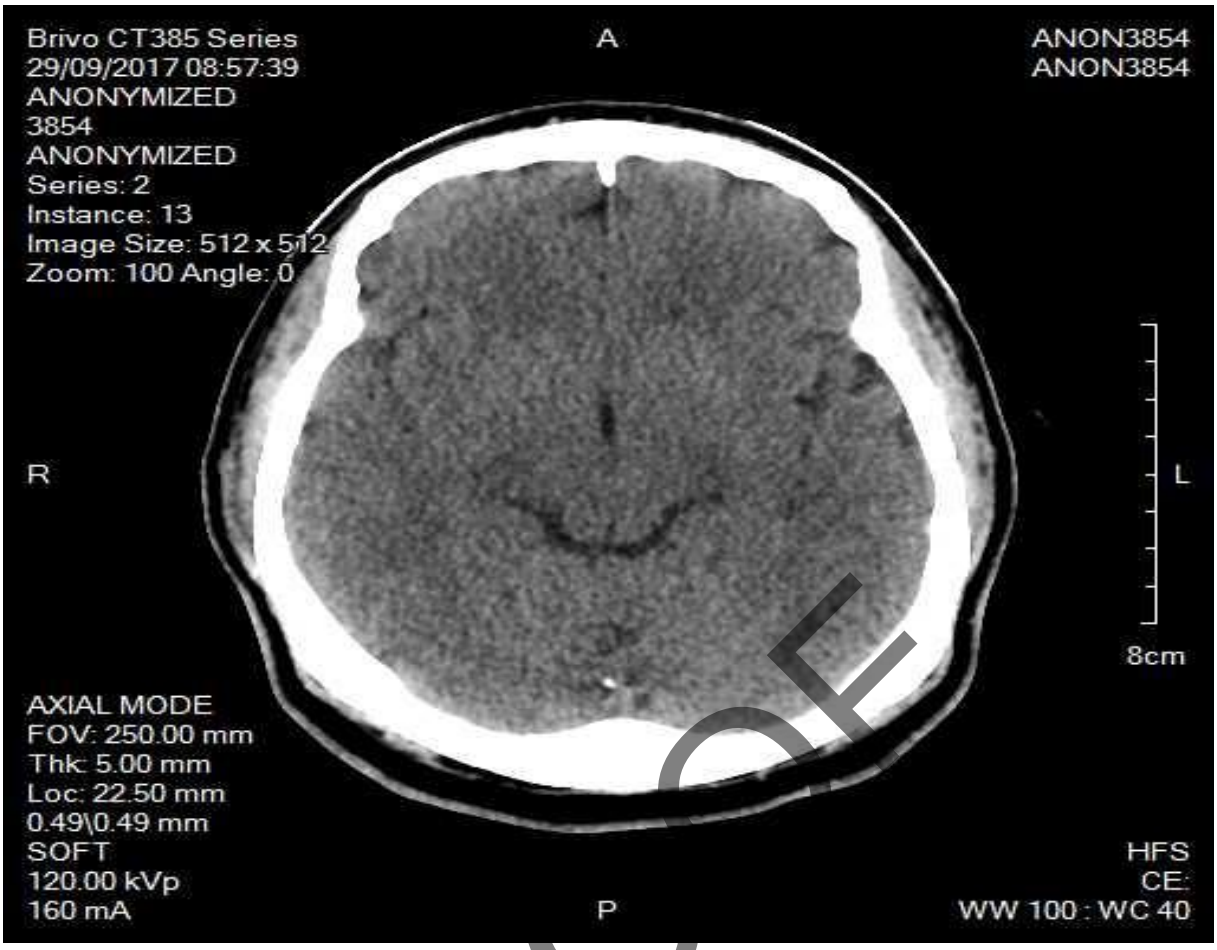

Figure 4. Paediatric head CT images without ring artefact

archived images of moderate paediatric hydrocephalus (Figure 2 a,b and 3), and establishes that significant differences exist in mean CTn values between ''ring'' bands of varying brightness observed (Tables 6 and 7). This presents a shade of gray since the CTn value stored in each ''ring'' band represents the average linear attenuation coefficient of the traversed tissue volume [2]. Changes in attenuation value for the same material are accounted for by results of interaction processes of x-radiation with matter through photon starvation and/or beam hardening, and this alters attenuation values significantly [2, 4, 15]. Also, following the x-ray linear travel path principle [16], these attenuation value alterations through photon starvation or beam hardening phenomena are relatively unidirectional and are assumed to be resolved within certain specific radial distance intervals from the image edge to the iso-centre as x-radiation passes through the subject [17- 20]. Therefore, within a certain range of volume or tissue thickness of a homogeneous or relatively homogeneous unit under study (paediatric hydrocephalus mimicking phantom and in paediatric moderate to severe hydrocephalus images), changes in attenuation are thus expected and are represented as regional areas of varied visually perceived brightness on the image(s). These visually perceived areas of varying intensity brightness on the images provide a visual manifestation of changes in CTn as the X-ray beam traveled over a distance in tissue along a linear path. The CTn value changes in an image along a linear path, thus influences image contrast, which, in combination with the physiology of the eye, constitutes factors that influence one's ability to distinguish between neighboring regions on a CT image [2].

In the heterogeneous unit (nil hydrocephalus paediatric head), the same principle of x-radiation interaction processes with matter, whether through photon starvation or beam hardening processes during image acquisition applies and differential attenuation values are also recorded. And these values also change

within a certain range(s) of volume or tissue thickness traversed by x-radiation from the image edge to the centre. But within a similar distance range traveled by x-radiation, there is tissue inhomogeneity due to the presence of mixed composition of brain tissue, blood vessels, and CSF [21]. This canceled out the formation of significant homogeneous intensity brightness within a certain distance range or tissue thickness upon x-radiation travel and thus, no ''ring'' track(s) or path(s) can be traced on the CT image formed. Rather, an image with subtle heterogeneous intensities, which is representative of the tissue attenuation coefficient of each brain constituent is seen (Figure 4).

5. Conclusion

Although defective tube and/or tube miscalibration have been implicated in the formation of a " ring " artefact in available literature, the results of this study suggest that ring artefact could be associated with hydrocephalus. However, changes in CTn with distance were not investigated in this study; thus, a new front for further research.

References

1- C. Godoy, P. Naidich, E. Marchiori, B. Assadourian, C. Leidecker, B. Schmidt and I.Vlahos, "Basic principles and post-processing techniques of dual-energy CT: illustrated by selected congenital abnormalities of the thorax.'' *J Thorac Imaging*, vol. 24, no. 2, pp. 152-9, (2009), doi: 10.1097/RTI.0b013e31819ca7b2. PMID: 19465844.

2- A. Penelope and W. Jerry, "*Farr's Physics for Medical Imaging,"* 2nd ed. London: Elsevier, pp. 207 – 216, (2008).

3- D. R Dance, S. Christofides, A.D.A. Maidment, I. D. McLean, and K.H. Ng, "Diagnostic Radiology Physics: a handbook for teachers and students." *Vienna: International Atomic Energy Agency (IAEA)*, pp. 257 – 287, (2014).

4- F. Barrett and K. Nicholas, "Artefacts in CT: Recognition and avoidance.'' *Radiographics*, vol. 24, no.6, pp.1679 – 1691, (2004), doi:10.1148/rg.246045065

5- S. Lai, H. Peng, and E. Yu, ''A new method for quickly correcting ring artifacts in CT image.'',*Symb J Clin Rehab Tiss Engr Resear*, vol. 15, no. 13, pp. 2412-2515, (2011), doi: 10.3969/j.issn.1673-8225.2011.13.031.

6- F. Boas and F. Dominik, "CT Artefacts: Causes and reduction techniques.", *Imaging Medicals*, vol.4, no. 2, pp. 229-240, (2012), doi:10.2217/iim.12.13

7- M. Walker, "Cerebrospinal fluid physiology: Problems and possibilities.", *J Clin Neurosurg, vol.* 58, pp. 123-145, (2011), doi: 10.1227/neu.0b013e3182270170. PMID: 21916129.

8- N. Czarniak, J. Kamińska, J. Matowicka-Karna and M. Koper-Lenkiewicz, "Cerebrospinal Fluid-Basic Concepts Review Biomed, vol.11, no. 5, pp. 1461, (2023), doi: 10.3390/biomedicines11051461. PMID: 37239132; PMCID: PMC10216641.

9- A. Hochstetler, J. Raskin and L. Blazer-Yost, "Hydrocephalus: historical analysis and treatment considerations." *Eur J Med Res*. vol. 27, no. 1, pp. 168, (2022), doi: 10.1186/s40001-022-00798-6. PMID: 36050779; PMCID: PMC9434947.

10- A. Mohammed, U. Anthony, A. Azuoma, and I. Hassan, "Comparative Stereological Analysis of Intracranial Volume Fractions among Patients with Brain Atrophy and Normal Pressure Hydrocephalus from a Nigerian Population.", *EJMED*, vol. 3, no. 2, pp. 192–196, (2021), doi: 10.24018/ejmed.2021.3.2.779.

11- W. Bonadio, "Pediatric lumbar puncture and cerebrospinal fluid analysis.'' *The Journal of Emergency Medicine*, vol. 46, no. 1, pp. 141-50, (2014), doi: 10.1016/j.jemermed.2013.08.056.

12- E. Lamb, S. Rent, J. Brannon, L. Greer, P. Ndey-Bongo, H. Cho, G. Greenberg, K. Benjamin Jr, H. Clark, R. Kumar, "Diagnostic Utility of Cerebrospinal Fluid White Blood Cell Components for the Identification of Bacterial Meningitis in Infants.'' *Journal of the Pediatric Infectious Diseases Society*, Vol. 26, no. 12, pp. 44-52, (2023). doi: 10.1093/jpids/piad087. PMID: 38146862; PMCID: PMC10750308.

13- H. Hasanzadeh and A. Abedelahi, "Introducing a simple tissue equivalent anthropomorphic phantom for radiation dosimetry in diagnostic radiology and radiotherapy.", *Archives of Advances in Biosciences,* vol. 2, no. 4, (2011), doi.org/10.22037/jps.v2i4.2718

14- W. James, E. Daniel. F. Ryan, T. Christopher and H. David, "Construction of anthropomorphic phantoms for use in dosimetry studies.'' *Journal of Applied Clinical Medical Physics*, *vol.* 10, no. 3, pp. 195-204, (2009), doi: 10.1120/jacmp.v10i3.2986. PMID: 19692982; PMCID: PMC5720556.

15- H. Jung, "Basic Physical Principles and Clinical Applications of Computed TomographyTomography." *Progress in Medical Physics*, Vol. 32, pp. 1-17, (2021), doi: 10.14316/pmp.2021.32.1.1.

16- Berger M, Yang Q, Maier A. X-ray Imaging. 2018 Aug 3. In: Maier A, Steidl S, Christlein V, *et al.*, editors. "Medical Imaging Systems: An Introductory Guide [Internet]." *Cham (CH): Springer*; 2018. Chapter 7. Available from: https://www.ncbi.nlm.nih.gov/books/NBK546155/ doi: 10.1007/978-3-319-96520-8_7

17- J. Cesar, A. Schueler, E. Zink, R. Daly, P. Taubel, L. Jorgenson, “Artefacts found in computed radiography.” *British Journal of Radiology*, (2001)., 74(878):195-202, doi: 10.1259/bjr.74.878.740195. PMID: 11718396.

18- Y. Mehran and M. Zohre, “Metal artifact reduction in spiral fan-beam CT using a new sinogram segmentation scheme,” *Journal of X-Ray Science and Technology*, vol. 25, no. 5, pp. 1-13, (2017). doi:10.3233/XST-16224.

19- F. Alzain, N. Elhussein, A. Fadulelmulla, M. Ahmed, E. Elbashir, A.Elamin, “Common computed tomography artifact: source and avoidance.’’ *The Egyptian Journal of Radiology and Nuclear Medicine*, vol. 52, pp. 151, (2021), doi:10.1186/s43055-021-00530-0

20- E. Mohamed, E. Abdelmajid, P. Francoise, A. Mustapha, “Detection of ring artifacts in computed tomographic images,’’ *Journal of Theoretical and Applied Information Technology*, vol. 94 no. 1, pp.84-94, (2016).

21- A. Schmidt, F. Despas, A. Pavy-Le, Z. Czosnyka, D. Pickard, K. Rahmouni, A. Pathak and M. Senard, “Intracranial Pressure Is a Determinant of Sympathetic Activity" *Frontiers in Physiology*, Vol. 9, pp.11, (2018). doi: 10.3389/fphys.2018.00011